# Nanoscale

Accepted Manuscript


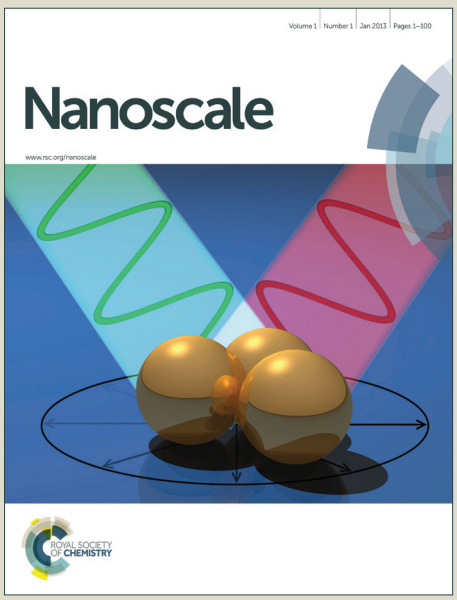





ROYAL SOCIETY OF CHEMISTRY

www.rsc.org/nanoscale

Cite this: DOI: 10.1039/c0xx00000x

www.rsc.org/xxxxxx

ARTICLE TYPE

# Multilevel memristor effect in metal-semiconductor core-shell nanoparticles: tested by scanning tunneling spectroscopy

**Sudipto Chakrabarti and Amlan J. Pal***

*Department of Solid State Physics, Indian Association for the Cultivation of Science, Jadavpur, Kolkata 700032, India.*

*E-mail: sspajp@iacs.res.in; Fax: +91-33-24732805; Tel: +91-33-24734971*

***Received (in XXX, XXX) Xth XXXXXXXXX 20XX, Accepted Xth XXXXXXXXX 20XX***

**DOI: 10.1039/b000000x**

We grow gold (Au) and copper-zinc-tin-sulfide (CZTS) nanocrystals and Au-CZTS core-shell nanostructures having gold in the core and the semiconductor in the shell-layer through a high-temperature colloidal synthetic approach. Following usual characterization, we form their ultrathin-layers to characterize the nanostructures in an ultrahigh-vacuum scanning tunneling microscope. Scanning tunneling spectroscopy of individual nanostructures show memristor effect or resistive switching from a low- to a high-conducting state upon application of a suitable voltage pulse. The Au-CZTS core-shell nanostructures in addition evidence multilevel memristor effect with the nanostructures undergoing two transitions in conductance at two magnitudes (of voltage pulse). We study the reproducibility, reversibility, and retentivity of the multilevel memristors. From the normalized density of states (NDOS), we infer that the memristor effect is correlated to a decrease in the transport gap of the nanostructures. We also infer that memristor effect occurs in nanostructures due to an increase in the density of available states upon application of a voltage pulse.

## 1. Introduction

After Leon Chua discovered the possible existence of memristor in 1971[1] from the symmetry of Maxwell's electromagnetic equations, the electronic science was revolutionized. Researchers across the globe looked for a range of materials whose electrical resistance would depend on the history of current that had previously flew through the material. With the device remembering its history even when the electric power was turned off, such memristors have became an element for resistive-switching memory applications.[2,3]

Materials used for memristors comprise of a wide range of direct[4,5] and indirect bandgap[6-8] (inorganic) semiconductors apart from conjugated polymers and organic semiconductors[3,9,10] and metals[11,12] and metal oxides.[4-6,13-15] The choice of materials naturally depended on the parameters used to "read" the states of memory elements. Although memristors are commonly read by measuring their electrical conductivity, the state of memory-elements can also be read by optical, dielectric and magnetic readouts.[9,16,17] Apart from the search for novel materials, researchers also targeted their lower-dimensional forms.[4-6,11-14] The apparent aim was to increase the density of memory-elements, although a fewer reports are available on probing of individual or single nanostructures. It is quite obvious that to achieve high-density memory from memristors, an isolated low-dimensional structure has to be probed. In a few such reports in this direction, conductive atomic force microscopy (c-AFM) or scanning tunneling microscopy (STM) has been employed to switch organic compounds or individual nanostructures and also to read the state of the active materials.[18-26] Apart from the ability to target individual nanostructures, a major advantage of the microscopies is that filament formation[27] can be ruled out due to the noncontact mode of write and read processes.

In probing memristors based on nanostructures with STM, we went ahead in choosing core-shell systems. In contrast to memristor phenomenon in simple nanoparticles, we aimed to choose metal-semiconductor core-shell nanoparticles in order to achieve a multilevel conductivity that in turn would increase the density of memory elements. In this work, we chose gold nanocrystals as the core encapsulated with a shell layer of a high-dielectric quaternary semiconductor. We recorded scanning tunneling spectroscopy (STS) and then evaluated density of states (DOS) of such core-shell nanoparticles to evidence memristor-based multilevel memory through STM.

## 2. Experimental section

**A. Materials.** Copper(II) acetate, zinc(II) acetate, tin(II) chloride dihydrate ($SnCl_2{\cdot}2H_2O$), copper(II) chloride dihydrate ($CuCl_2{\cdot}2H_2O$), zinc(II) chloride dihydrate ($ZnCl_2{\cdot}2H_2O$), and sulfur powder were purchased from Loba Chemie Pvt. Ltd. Oleylamine, 1-dodecanethiol, tin(IV) chloride ($SnCl_4$) and gold(III) chloride trihydrate ($HAuCl_4{\cdot}3H_2O$) were purchased from Sigma-Aldrich Chemical Company. All the chemicals were used without further purification.

**B. Growth of copper-zinc-tin-sulfide (CZTS) nanoparticles.** To grow nanoparticles of quaternary $Cu_2ZnSnS_4$, we have followed a reported route with certain modifications.[28,29] In short, $CuCl_2{\cdot}2H_2O$ (1 mM), $ZnCl_2{\cdot}2H_2O$ (0.5 mM), and sulfur (2 mM) were dissolved in 20 mL of oleylamine. The reaction flask was thoroughly degassed under a continuous stirring condition for 30 min followed by addition of 0.06 mL of $SnCl_4$ (0.5 mM). Temperature of the reaction flask was then raised to 120 ºC

followed by further stirring and degassing for 30 min. Finally, the temperature was raised to 180 ºC to initiate the growth of CZTS nanocrystals. After 1 h, the reaction was stopped by lowering the temperature to 80 ºC; 5 mL of anhydrous toluene was added to the flask to stabilize the nanocrystals. Finally, CZTS nanocrystals were precipitated by adding 2-propanol and separated by centrifugation at 8000 rpm for 15 min. Long-chain oleylamine capped CZTS nanocrystals were then redispersed in toluene for further use.

**C. Growth of gold nanocrystals**. To grow gold nanocrystals, $HAuCl_4 \cdot 3H_2O$ was dissolved in 5 mL oleylamine kept in a reaction flask to form 0.5 mM solution. The solution was degassed in nitrogen environment under a vigorous stirring condition. Temperature of the reaction flask was then raised to 120 ºC. In 10 min, the color of the solution turned wine-red implying formation of gold nanocrystals. The nanoparticles were separated by adding excess ethanol in chloroform followed by centrifugation at 8000 rpm for 5 min. They were redispersed in chloroform for further use.

**D. Growth of Au-CZTS core-shell nanostructures.** For a typical synthesis of core-shell nanostructures with gold nanocrystals as a core and a shell of CZTS, we have followed a reported route with certain modifications.[30] In a typical synthesis, copper acetate (1.8 mM), zinc acetate (1.2 mM), and tin chloride (1 mM), were added separately in 4 mL of oleylamine. The solution was degassed for 2 h. The temperature of the flask was then raised to 120 ºC; at this stage gold nanocrystals capped with oleylamine were swiftly injected into the reaction flask under a continuous stirring condition. After a couple of minutes, 400 μL of dodecanethiol, as a source of sulfur, was added to the flask. Temperature of the flask was then raised to 280 ºC to allow formation of a CZTS shell-layer. After 30 min, the reaction was stopped by cooling the flask down to room temperature. The core-shell nanostructures were precipitated by adding a mixture of chloroform and ethanol; they were separated by centrifugation at 8000 rpm for 15 min. Finally the Au-CZTS core-shell nanostructures were redispersed in chloroform and stored at 4 ºC under a dark condition for future use.

**E. Characterization of the nanoparticles.** The nanostructures were characterized by UV–visible optical absorption spectroscopy, transmission electron microscopy (TEM), high resolution TEM (HR-TEM), energy dispersive X-ray analysis (EDXA), X-ray diffraction (XRD) analysis, and X-ray photoelectron spectroscopy (XPS). The measurements were carried out with Shimadzu UV-2550 Spectrophotometer, JEM 2100F Jeol TEM, Bruker D8 Advanced X-ray Powder Diffractometer, and an XPS instrument (Omicron: Serial number 0571), respectively.

**F. Film formation of nanostructures: STM measurements.** Since we would be recording tunnel-conductance to probe resistive-switching or memristor effect of isolated nanostructures through scanning tunneling microscopy, we formed ultrathin films of the nanoparticles on arsenic-doped silicon <111> electrodes, which had a resistivity of 5-10 mΩ·cm. The wafers were pre-cleaned by a standard protocol to remove any organic contaminants followed by a treatment with dilute hydrofluoric acid in order to remove the native oxide on the surface. To form an ultrathin layer of the nanostructures, their dispersed solution in chloroform was spun immediately on the electrodes at 3500 rpm. The films were inserted into the STM chamber following a usual procedure.

STM measurements were carried out with a PAN-style Ultra-High Vacuum STM (UHV-STM) manufactured by M/s RHK Technologies, USA. The base pressure of the microscope chamber was kept at $2.0 \times 10^{-10}$ Torr. Platinum/iridium (Pt/Ir, 80%/20%) wires which were cut mechanically, were used at STM tips to record STS and tunneling current versus voltage (*I-V*) characteristics of the ultrathin films of different nanostructures. Bias was applied to the substrate-electrode. During the approach of the tip, a preset current was achieved at 2.0 V through a feedback loop of the STM controller. Imaging of the nanostructures and measurement of tunneling current were carried out on many different points on each ultrathin film to check reproducibility of the results. Tunneling current was recorded with a voltage sweep between -2.5 and 2.5 V in both sweep directions.

**G. Electrical bistability of nanostructures.** After approach of the tip, we aimed to characterize the nanostructures for a possible memristor effect. To observe resistive-switching in individual nanostructures, feedback loop of the STM controller was put to a disabled-mode, so that the tip-to-nanostructure distance remained unaltered during the measurement of tunnel-conductance of a nanostructure. Tunnel-conductance of a pristine layer was first recorded in the -2.5 to 2.5 V region. A voltage-pulse of suitable magnitude was then applied; tunneling current was again measured to look for any change in tunnel-conductance. Since the tip-to-nanostructure distance remained the same, a change in the conductance would be due to the memristor effect of individual nanostructures. We varied the magnitude of voltage pulse between 3.0 to 9.0 V in a step of 0.5 V, since it has been observed that a higher-conducting state appeared due to application of a positive voltage pulse. The lower-conducting pristine state was reinstated by applying a reverse voltage (of -10.5 V) before measuring the tunneling current. Measurements were also carried out by varying the width of the voltage-pulse between 10 to 100 ms. Density of states (DOS) were calculated by numerical derivative of the *I-V* characteristics.

## 3. Result and discussion

### A. Characteristics of the nanostructures.

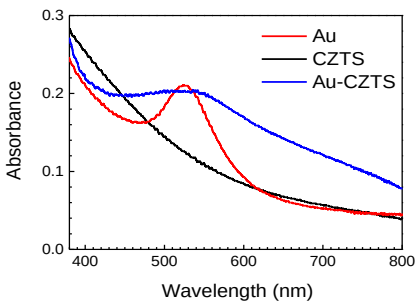


**Fig 1.** Optical absorption spectra of gold and CZTS nanocrystals and Au-CZTS core-shell nanostructures in dispersed solutions.

Optical absorption spectra of CZTS and gold nanocrystals, along

with Au-CZTS core-shell nanostructures are shown in Fig. 1. The spectra of gold and CZTS nanocrystals matched the reported results of the respective materials of similar diameter.[30] The band of the former nanostructure appeared due to plasmon absorption of colloidal gold nanoparticles. With formation of CZTS shell layer around gold nanocrystals, the band of gold became screened and underwent a red-shift of 19.5 nm apparently due to the low bandgap and high dielectric constant of the shell material.[31]

Fig. 2 shows TEM and HR-TEM images of gold and CZTS nanocrystals and Au-CZTS core-shell nanostructures. The TEM images of gold and CZTS nanocrystals show a high degree of monodispersivity. A histogram of diameter distribution calculated from more than 50 nanocrystals in each of the cases is also presented in the figure. Average diameter of gold and CZTS turned out to be 15 and 10 nm, respectively. In the HR-TEM images, an interplanar spacing of 0.24 nm for both the nanocrystals was observed that corresponded to (111) and (111) planes of cubic gold and kersterite-type tetragonal phase of CZTS, respectively.

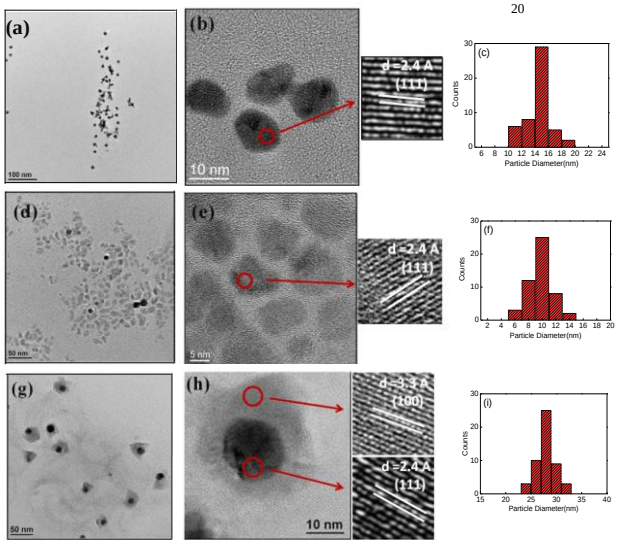


**Fig. 2.** TEM, HR-TEM, and histogram of diameter distribution of gold nanocrystals (*a* to *c*), CZTS nanocrystals (*d* to *f*), and Au-CZTS core-shell nanostructures (*g* to *i*).

From the TEM image of Au-CZTS core-shell nanostructures, formation of a shell layer on gold nanoparticles is clearly visible. The spherical gold nanoparticles were completely embedded with the CZTS shell layer. The figure shows that with the diameter of gold nanoparticles being 15 nm the average shell thickness being about 13 nm, the total diameter of the core-shell nanostructures turned out to be 28 nm. The diameter matches with the value obtained from the histogram of diameter distribution as calculated from the measurement of the diameter of 100 or more particles. Such a histogram is shown in a part of Fig. 2. HR-TEM images of the nanostructures show a high degree of crystalline nature of both the core and the shell materials. The measured interplanar spacing of 0.24 and 0.33 nm of the material in the core and in the shell corresponded to (111) and (100) planes of cubic gold and wurtzite CZTS, respectively. The results are in concurrence with the reported results.[30]

Fig. S1 in the Supplementary Information shows elemental composition of CZTS nanocrystals and Au-CZTS core-shell nanostructures. The spectrum of the latter nanocrystals shows that the peaks corresponding to gold appeared only in the Au-CZTS system. XRD patterns of gold, CZTS, and Au-CZTS nanostructures are presented in Fig. S2 in the Supplementary Information. The diffraction peaks of gold nanocrystals represented a cubic lattice (JCPDS file #04-0784). The patterns of CZTS nanocrystals could be indexed to kersterite type tetragonal phase (JCPDS file #26-0575) of the material. Diffraction peaks of the core-shell systems include patterns of CZTS nanocrystals in their wurtzite phase,[30] apart from the patterns corresponding to the cubic lattice of gold nanocrystals. Any secondary phase due to binary sulfides did not appear in the spectra.

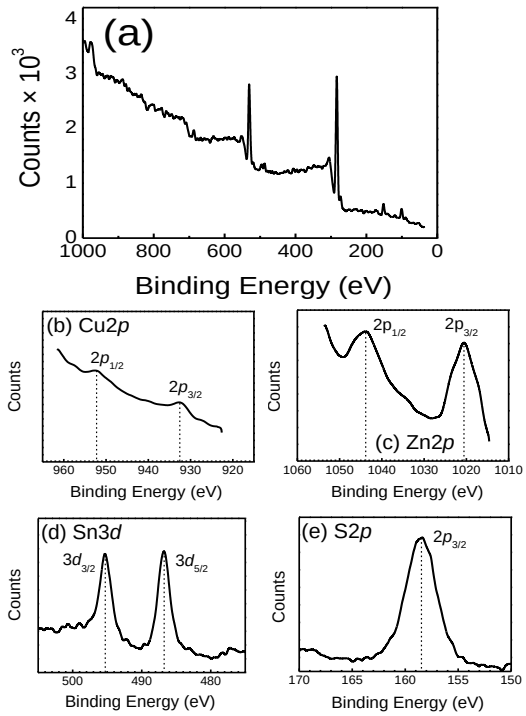


**Fig. 3.** (a) Full-range XPS spectrum of Au-CZTS nanostructures. High-resolution XPS spectra of Cu2*p*, Zn2*p*, Sn3*d*, and S2*p* of the nanostructure are shown in (b) – (e) in sequence.

We have carried out XPS studies to obtain information about the valence state and elemental composition of Au-CZTS core-shell nanostructures. The full-scan spectrum of the nanostructure is presented in Fig. 3, which confirms the presence of copper, zinc, tin, and sulfur. The absence of any peak corresponding to the valance state of gold confirms a complete coverage of gold nanoparticles with the semiconductor layer and also rules out the presence of any gold atoms on the surface. High-resolution spectra in small energy regions are also presented in Fig. 3. Here, the binding energies obtained in the XPS analyses were corrected with reference to C1*s* peak at 284.5 eV. As can be seen from the figure, the spectrum for Cu2*p* was resolved into $2p_{3/2}$ and $2p_{1/2}$ peaks at 932.6 and 952.2 eV, respectively. The binding energy splitting of Cu2*p* was about 19.6 eV which confirmed the presence of Cu(I) state in the material. Similarly the spectrum of Zn2*p* was resolved into $2p_{3/2}$ and $2p_{1/2}$ peaks located at 1020.6 and 1043.9 eV, respectively. The binding energy splitting of the state was about 23.3 eV which confirms the presence of Zn(II)

state. The spectrum of Sn3*d* was resolved into $3d_{5/2}$ and $3d_{3/2}$ peaks at 486.8 for and 495.4 eV, respectively, with a binding energy splitting of 8.6 eV. Here, the binding energy matched well with Sn(IV) state and thus confirming its presence in the Au-CZTS core-shell nanostructures. Finally, the spectrum of sulfur yielded a peak at 158.5 eV which corresponded to the $2p_{3/2}$ state of $S^{2-}$. The high-resolution XPS spectra hence infer formation of $Cu_2^+Zn^{2+}Sn^{4+}S_4^{2-}$ in the nanostructures.

**B. Memristor effect in nanostructures: tested by scanning tunneling spectroscopy.** We have characterized ultrathin films of the nanocrystals by Pt/Ir tip of a STM. Tip approaching current was kept low (0.7 nA at 2.0 V) to ensure that the tip does not influence the states of the nanostructures. The lower-dimensional materials that we chose for this purpose are gold and CZTS nanocrystals and Au-CZTS core-shell nanostructures. For each of the ultrathin-films of the three materials, we first recorded their surface topographies (inset of Figs. 4a-c). We then recorded tunneling current versus voltage characteristics (a) of the pristine film, (b) after application of a positive voltage pulse which switches the nanostructures to a higher conducting state, and (c) after application of a negative voltage pulse (-10.5 V) reinstating the initial low-conducting state. Magnitude of the positive voltage pulse was varied between 3.0 and 9.0 V in a step of 0.5 V to look for a variation in tunneling current or the number of possible (tunnel) conducting-states in the nanostructures. Width of the voltage pulse was in general 10 ms; it was also varied in the 10-100 ms range in separate set of experiments. All the measurements were carried out with the feedback-loop in a disabled condition, so that, when the tunnel-conductance of a nanostructure changes upon application of a voltage pulse, the tip-to-nanocrystal distance is not adjusted to maintain the tip-approaching current.

*I-V* characteristics of the three nanostructures have been clubbed in Figs. 4(a) to 4(c). The figures show that for gold and CZTS nanocrystals, the *I-V*s show two types of characteristics: a low and a high level of current at each voltage. For Au-CZTS core-shell nanostructures, three such *I-V*s were observed. The *I-V* characteristics did not change when the magnitude of voltage pulse was low and below a particular value. When the voltage pulse had a magnitude beyond a threshold value ($V_{Th}$), a new set of *I-V* characteristics could be observed that yielded a higher (magnitude of) current at any voltage. The jump in current (at a voltage) upon application of a voltage pulse of suitable magnitude infer memristor effect in individual gold and CZTS nanocrystals since the nanostructures were probed by a STM tip. The Au-CZTS core-shell nanostructures evidenced two such jumps in current inferring multilevel tunnel-conductance in the memristor. The memristor effect can best be viewed if the current at a low voltage (say 2.5 V), as measured during the record of *I-V* characteristics, is plotted as a function of the magnitude of voltage pulse that preceded the measurement of tunneling current. The Fig. 4(d) shows such a plot for all the three nanostructures. The plots bring out a clear memristor effect in gold and CZTS nanocrystals with two tunnel-conductance states. The threshold voltage required to switch the nanostructures was 6.0 and 6.5 V for the metal and the semiconductor, respectively. For the metal-semiconductor core-shell nanostructures, the two-step switching or multilevel memristor effect is clearly visible in Fig. 4(d). The two threshold voltages turned out to be 5.5 and 8.5 V with a level of accuracy of 0.5 V which was the step used in varying the magnitude of voltage pulse.

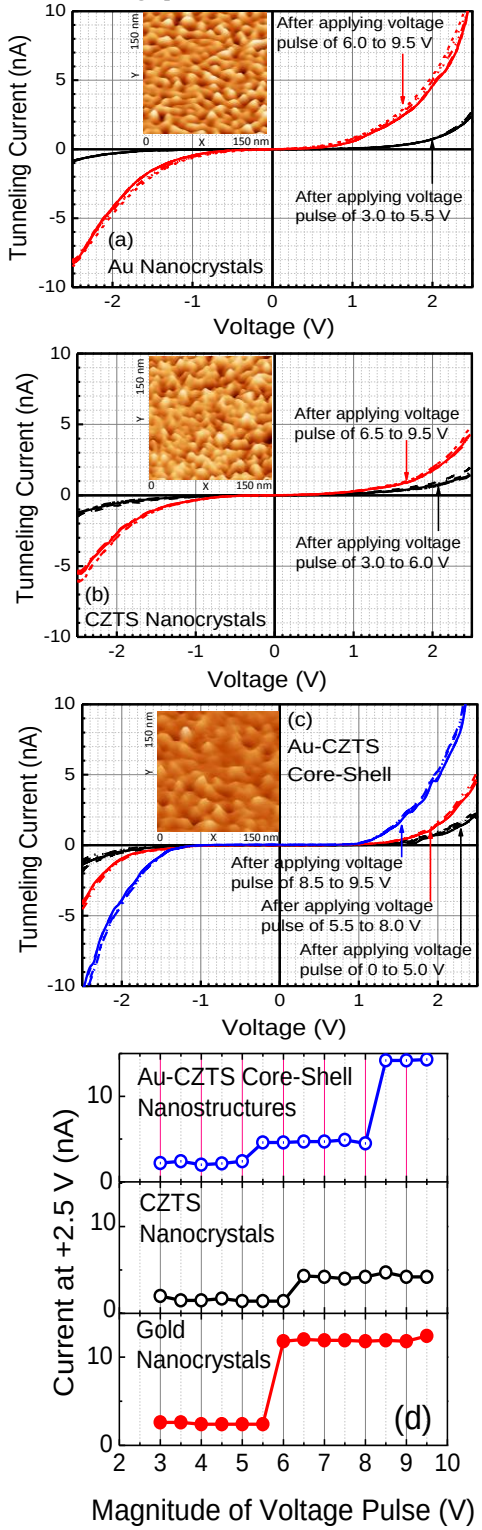


**Fig. 4.** Current-voltage characteristics of (a) gold and (b) CZTS nanocrystals and (c) Au-CZTS core-shell nanocrystals after application of a voltage pulse of different amplitudes. (d) Current at +2.5 V for all the nanostructures as a function of magnitude of voltage pulse that preceded the measurement of tunneling current versus voltage characteristics. Surface topographies of ultra-thin films are shown in the respective insets.

We also varied width of the voltage pulse that switches the memristors. To do so, we varied the width from 10 to 100 ms. *I-V* characteristics of the three nanostructures before and after application of the voltage pulse are shown in Fig. S3 in the Supplementary Information. In all the memristors, the tunnel-conductance switched upon application of a voltage pulse of suitable amplitude. The invariance of memristor effect with the width of voltage pulse can be summed up as a plot of current at a voltage (say +2.5 V), as measured during the record of *I-V* characteristics, as a function of the width of voltage pulse that preceded the voltage sweep to record the characteristics.

### C. Reproducibility, reversibility, and retention time of (multilevel) memristors

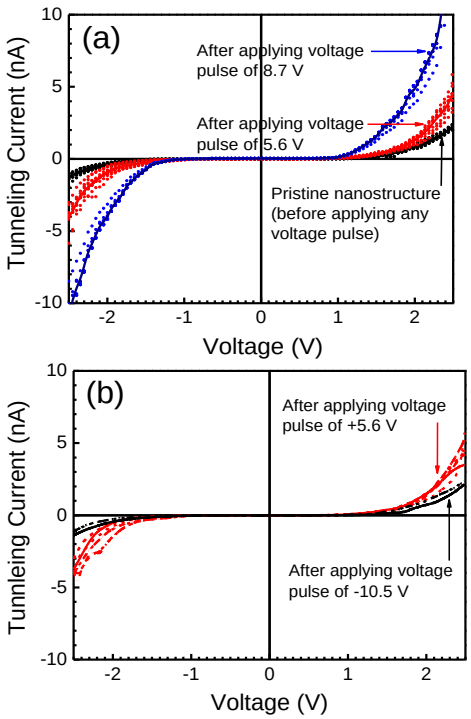


**Fig. 5.** Current-voltage characteristics of Au-CZTS core-shell nanostructures (a) before and after application of 5.6 or 8.7 V voltage pulse and (b) after application of a voltage pulse of +5.6 V and -10.5 V over many cycles.

To check the reproducibility of the memristor effect in the nanostructures, we carried out measurements at many different points on their ultrathin films. While the characteristics of gold and CZTS nanocrystals at many different points are presented in Fig. S4 in the Supplementary Information, *I-V*s of Au-CZTS nanostructure at 10 different points are shown in Fig. 5(a). At each point, we recorded tunneling current before and after application of a voltage pulse of either +5.6 or +8.7 V. While the *I-V*s of pristine nanostructures represent their low-conducting state, the +5.6 and +8.7 V voltage pulses induced the first and the second high-conducting states, respectively. The results presented in Fig. S4 in the Supplementary Information and Fig. 5(a) hence show the reproducible nature of memristor effect in gold, CZTS, Au-CZTS nanostructures. We also repeated such measurements in many cycles. The reversibility of the results is presented in Fig. S4 in the Supplementary Information for gold and CZTS nanocrystals; similarly, the Fig. 5(b) represents such measurements for Au-CZTS core-shell nanostructures. Here, we recorded tunneling current after application of a voltage pulse of +5.6 V and -10.5 V over many cycles. While the +5.6 V induced a high-conducting state, the -10.5 V pulse reinstated the initial low-conducting state. The results hence inferred reproducibility and reversibility of (multilevel) memristors in (core-shell) nanostructures.

To estimate the retention time of the high-state(s), we probed them continuously by measuring *I-V* characteristics in the -2.5 to +2.5 V range. For gold and CZTS nanocrystals, we applied a positive voltage pulse (+7.0 and +7.5 V, respectively) before measuring the *I-V* characteristics over a period of time. The plots, as presented in Fig. S5 in the Supplementary Information show that the *I-V* characteristics remained invariant for at least 10 min. Current at 2.5 V as a function of time (insets of Fig. S5) also shows that the nanocrystalline memristors retained their high-state for a considerable period of time. For the Au-CZTS core-shell nanostructure, we applied a +6.0 or a +9.0 V pulse before measuring the *I-V* characteristics over the same period of time. The plot for current at a particular voltage as a function of time is shown for the two high states (Fig. 6). The results show that in Au-CZTS core-shell nanostructures, each of the two high-states could be retained for at least 10 min.

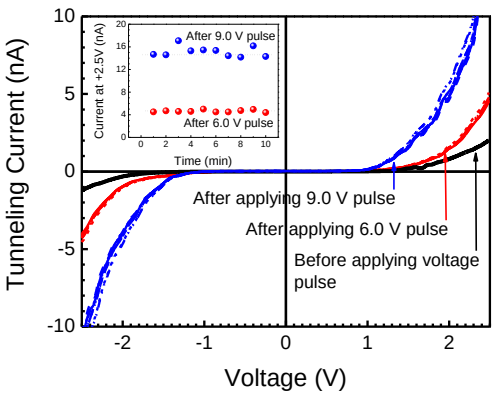


**Fig. 6**. Current-voltage characteristics of Au-CZTS core-shell nanostructures recorded for 10 times after application of a +6.0 or a +9.0 V pulse. *I-V* characteristics before applying a voltage pulse are also shown. Plots of current at +2.5 V (as obtained from the *I-V* characteristics) as a function of time for the two high-states are shown in the inset of the figure.

**D. Normalized density of states.** From STS, we have calculated the normalized density of states (NDOS) of the nanostructures in their different conducting states. Fig. 7 shows such plots for gold and CZTS nanocrystals before and after application of a voltage pulse that switches the nanostructures to their high-conducting state. For Au-CZTS core-shell nanostructures, we show NDOS in their pristine state and in two high-conducting states. The NDOS spectra provides the location of conduction and valence band-edges (CB and VB, respectively) in the form peaks in the positive or negative tip-voltages, respectively, at which electrons could be injected or withdrawn from the nanostructures. In the NDOS spectra of all the nanostructures, we observe that upon switching to a high-conducting state, the CB and VB edges shifted towards the Fermi energy, which is considered to be aligned at 0 V, and thereby decreasing the transport gap of the nanostructures. For

Au-CZTS nanostructures, the transport gap decreased in succession when the core-shell nanoparticles underwent a transition from their pristine to the first and then to the second high-conducting states. This is in contrast to one-step decrease in the transport gap in gold and CZTS nanocrystals upon application of a voltage pulse, which switches the nanostructures to their only high-conducting state.

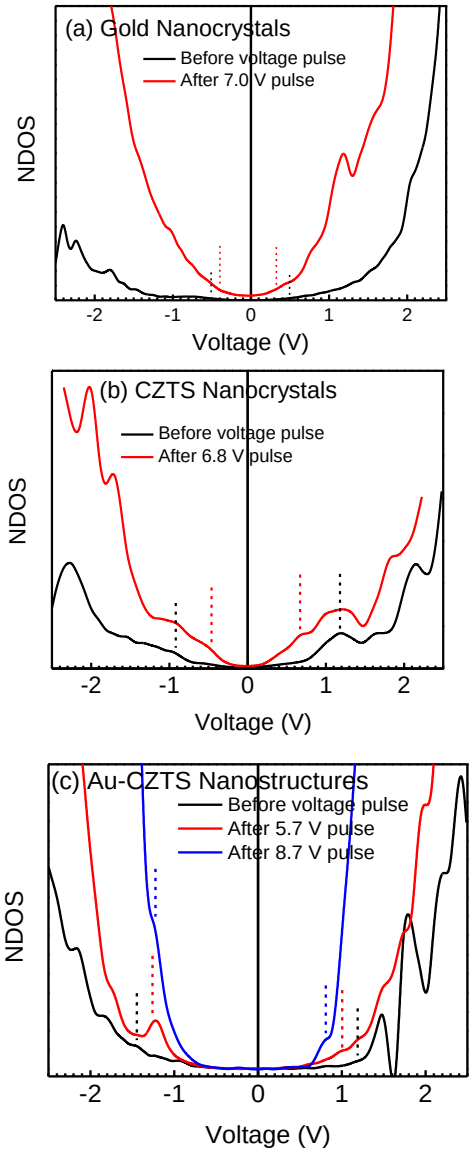


**Fig. 7.** Normalized Density of States (NDOS) spectra of (a) gold and (b) CZTS nanocrystals and (c) Au-CZTS core-shell nanostructures before and after application of a voltage pulse of amplitudes as specified in legends. Conduction and valence band band-edges (CB and VB, respectively) are marked by vertical lines in the positive and negative voltages, respectively, in each spectrum.

In addition to a decrease in the transport gap, the intensity of peaks in the NDOS spectra increased when the memristors underwent a transition from a low- to a high-conductance state. For Au-CZTS nanostructures, the intensity increased in succession for transitions to the first and then to the second high-conducting states. With the intensity in a NDOS spectrum related to the available states of a nanostructure, this implies that the memristor effect in gold and CZTS nanocrystals and the multilevel memristor effect in Au-CZTS core-shell nanostructures occurred due to an increase in the density of available states upon application of voltage pulse of suitable amplitudes. A component of the voltage pulse that actually falls on the nanostructure upon being matched to an energy level of it might have allowed tunneling of charge carriers to increase the density of available states leading to memristor effect in the individual nanostructures.

## Conclusions

In conclusion we have formed and characterized gold and CZTS nanocrystals and also Au-CZTS core-shell nanostructures having gold in the core and the semiconductor in the shell with STS. Upon application of a voltage pulse prior to recording the tunneling current, the nanostructures underwent a transition in conductance. For Au-CZTS core-shell nanostructures, two such transitions were observed evidencing two high conducting-states and hence multilevel memristor effect in each core-shell nanoparticles. Observation of multilevel memristor phenomenon is in contrast to simple resistive switching in nanoparticles. The memristor phenomena in the gold and CZTS nanocrystals and also in core-shell nanostructures were reproducible and reversible. We also evidenced retention of the high-state(s) of the memristors based on the nanostructures. From the normalized density of states (NDOS) and correspondingly the location of conduction and valence band edges of the nanostructures, we have observed that the transport gap decreased when the nanostructures underwent a transition from their pristine to the high-conducting state(s). From the NDOS, we could also infer that memristor effect in the individual nanostructures occurred due to an increase in the density of available states upon application of voltage pulse of suitable amplitudes.

**Supplementary information**. Additional figures. This material is available free of charge via the Internet at http://rsc.org.

**Acknowledgements.** The authors acknowledge funding from DST Nano Mission projects.

## Notes and references

1 L. O. Chua, *IEEE Trans. Circuit Theory*, 1971, **18**, 507-519.
2 Q. F. Xia, W. Robinett, M. W. Cumbie, N. Banerjee, T. J. Cardinali, J. J. Yang, W. Wu, X. M. Li, W. M. Tong, D. B. Strukov, G. S. Snider, G. Medeiros-Ribeiro and R. S. Williams, *Nano Lett.*, 2009, **9**, 3640-3645.
3 T. Berzina, A. Smerieri, M. Bernabo, A. Pucci, G. Ruggeri, V. Erokhin and M. P. Fontana, *J. Appl. Phys.*, 2009, **105**, 124515.
4 K. Nagashima, T. Yanagida, M. Kanai, K. Oka, A. Klamchuen, S. Rahong, G. Meng, M. Horprathum, B. Xu, F. W. Zhuge, Y. He and T. Kawai, *Jpn. J. Appl. Phys.*, 2012, **51**, 11PE09.
5 C. Li, G. J. Beirne, G. Kamita, G. Lakhwani, J. P. Wang and N. C. Greenham, *J. Appl. Phys.*, 2014, **116**, 114501.
6 W. I. Park, J. M. Yoon, M. Park, J. Lee, S. K. Kim, J. W. Jeong, K. Kim, H. Y. Jeong, S. Jeon, K. S. No, J. Y. Lee and Y. S. Jung, *Nano Lett.*, 2012, **12**, 1235-1240.
7 J. Yao, Z. Z. Sun, L. Zhong, D. Natelson and J. M. Tour, *Nano Lett.*, 2010, **10**, 4105-4110.

8 Y. J. Chen, K. C. Chang, T. C. Chang, H. L. Chen, T. F. Young, T. M. Tsai, R. Zhang, T. J. Chu, J. F. Ciou, J. C. Lou, K. H. Chen, J. H. Chen, J. C. Zheng and S. M. Sze, *IEEE Electron Device Lett.*, 2014, **35**, 1016-1018.

9 H. S. Majumdar, A. Bolognesi and A. J. Pal, *J. Phys. D-Appl. Phys.*, 2003, **36**, 211-215.

10 B. Mukherjee, S. K. Batabyal and A. J. Pal, *Adv. Mater.*, 2007, **19**, 717-722.

11 W. L. Leong, P. S. Lee, A. Lohani, Y. M. Lam, T. Chen, S. Zhang, A. Dodabalapur and S. G. Mhaisalkar, *Adv. Mater.*, 2008, **20**, 2325-2331.

12 J. S. Lee, *Gold Bull.*, 2010, **43**, 189-199.

13 R. K. Gupta, S. Krishnamoorthy, D. Y. Kusuma, P. S. Lee and M. P. Srinivasan, *Nanoscale*, 2012, **4**, 2296-2300.

14 Y. T. Lee, S. R. A. Raza, P. J. Jeon, R. Ha, H. J. Choi and S. Im, *Nanoscale*, 2013, **5**, 4181-4185.

15 Y. C. Yang, S. Choi and W. Lu, *Nano Lett.*, 2013, **13**, 2908-2915.

16 A. Emboras, I. Goykhman, B. Desiatov, N. Mazurski, L. Stern, J. Shappir and U. Levy, *Nano Lett.*, 2013, **13**, 6151-6155.

17 S. Krause, L. Berbil-Bautista, G. Herzog, M. Bode and R. Wiesendanger, *Science*, 2007, **317**, 1537-1540.

18 K. Takimoto, H. Kawade, E. Kishi, K. Yano, K. Sakai, K. Hatanaka, K. Eguchi and T. Nakagiri, *Appl. Phys. Lett.*, 1992, **61**, 3032-3034.

19 A. S. Blum, C. M. Soto, C. D. Wilson, C. Amsinck, P. Franzon and B. R. Ratna, *IEEE Trans. Nanobiosci.*, 2007, **6**, 270-274.

20 B. C. Das, S. K. Batabyal and A. J. Pal, *Adv. Mater.*, 2007, **19**, 4172-4176.

21 A. K. Rath and A. J. Pal, *Org. Electron.*, 2008, **9**, 495-500.

22 M. H. Lee and C. S. Hwang, *Nanoscale*, 2011, **3**, 490-502.

23 C. Moreno, C. Munuera, X. Obradors and C. Ocal, *Beilstein J. Nanotechnol.*, 2012, **3**, 722-730.

24 O. A. Ageev, Y. F. Blinov, O. I. Il'in, A. S. Kolomiitsev, B. G. Konoplev, M. V. Rubashkina, V. A. Smirnov and A. A. Fedotov, *Tech. Phys.*, 2013, **58**, 1831-1836.

25 J. C. Hou, S. S. Nonnenmann, W. Qin and D. A. Bonnell, *Adv. Funct. Mater.*, 2014, **24**, 4113-4118.

26 A. Gambardella, M. Prezioso and M. Cavallini, *Sci Rep*, 2014, **4**, 4196.

27 S. Ssenyange, H. J. Yan and R. L. McCreery, *Langmuir*, 2006, **22**, 10689-10696.

28 C. Steinhagen, M. G. Panthani, V. Akhavan, B. Goodfellow, B. Koo and B. A. Korgel, *J. Am. Chem. Soc.*, 2009, **131**, 12554-12555.

29 S. C. Riha, B. A. Parkinson and A. L. Prieto, *J. Am. Chem. Soc.*, 2011, **133**, 15272-15275.

30 E. Ha, L. Y. S. Lee, J. C. Wang, F. H. Li, K. Y. Wong and S. C. E. Tsang, *Adv. Mater.*, 2014, **26**, 3496-3500.

31 C. Persson, *J. Appl. Phys.*, 2010, **107**, 053710.

Cite this: DOI: 10.1039/c0xx00000x

www.rsc.org/xxxxxx

**ARTICLE TYPE**

Table of contents

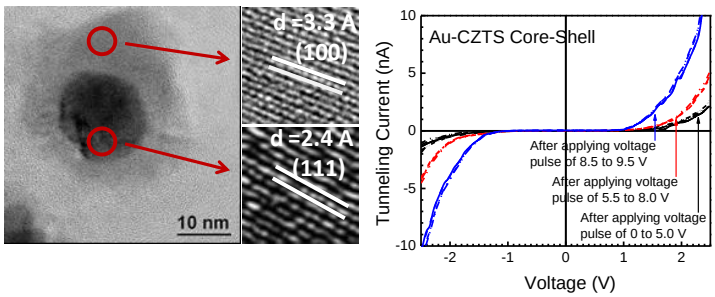


Scanning tunneling spectroscopy experiments of Au-CZTS metal-semiconductor core-shell nanoparticles reveal multilevel memristor effect. Voltage pulse of suitable magnitudes were applied to achieve two high-conducting states.